Talanta 83 (2011) 1386–1391

Contents lists available at ScienceDirect

Talanta

journal homepage: www.elsevier.com/locate/talanta

A novel glucose sensor based on ordered mesoporous carbon–Au nanoparticles nanocomposites

Lixia Wang, Jing Bai, Xiangjie Bo, Xiaoliang Zhang, Liping Guo*

Faculty of Chemistry, Northeast Normal University, Renmin Street 5268, Changchun, Jilin 130024, PR China

ARTICLE INFO

Article history:
Received 3 August 2010
Received in revised form 9 November 2010
Accepted 11 November 2010
Available online 18 November 2010

Keywords:
Au nanoparticles
Ordered mesoporous carbon
Direct electron transfer
Glucose oxidase
Glucose biosensor

ABSTRACT

Ordered mesoporous carbon–Au nanoparticles (OMC–Au) nanocomposites were synthesized by a one-step chemical reduction route. Due to the large surface area and high conductivity of OMC, good biocompatibility of OMC and Au nanoparticles, a mediator-free glucose biosensor was fabricated by immobilizing glucose oxidase (GOD) on the OMC–Au nanocomposites modified glassy carbon (GC) electrode. Direct electron transfer between GOD and the electrode was achieved and the electron transfer rate constant (k_s) was calculated to be 5.03 s^{-1}. The Michalis–Menten constant (K_M^{app}) value of GOD immobilized on the OMC–Au/GC electrode surface was found to be 0.6 mM. The glucose biosensor exhibits a linear range from 0.05 to 20.0 mM. This biosensor also shows good reproducibility, excellent stability and the negligible interferences from ascorbic acid and uric acid.

1. Introduction

The direct electrochemistry of redox proteins has received considerable attention in recent years. It is of theoretical and practical significance in biology, analytical chemistry, and other fields of science. It would elucidate their metabolic pathways in real biological systems and establish a foundation for constructing the third-generation biosensors without mediators [1–3]. Owing to the deep embedding of the redox center into the large three dimensional structures of enzyme molecules, the direct electron transfer (DET) between the redox proteins and the bare electrode is difficult to be realized [4]. Thus, it is of great interest in facilitating the DET and accelerating the electron exchange between the enzyme redox center and the electrode. In recent years, lots of biocompatible nanomaterials have been utilized to immobilize redox proteins and improve the electron transfer of biocatalytic processes. For the treatment and control of diabetes, the glucose oxidase (GOD)-based glucose biosensors have been widely studied [5–16]. The GOD has been immobilized on various nanomaterials, including carbon nanotubes [6,7], gold nanoparticles [8–10], ZnO nanorods [11] and ordered mesoporous material [12–17].

Recently, Au nanoparticles (AuNPs) have attracted significant attention in immobilizing of redox proteins because of their nano-scaled dimension effect [18], high surface area and good biocompatibility. AuNPs can also provide a microenvironment similar to that of redox proteins in native systems and reduce the insulating effect of the protein shell for the DET, which are essentially important for the achievement of direct electrochemistry of redox enzymes [19]. Indeed, Luo et al. [20] and Luckarift et al. [21] have shown that GOD could maintain its enzymatic and electrochemical activities when it was immobilized on AuNPs. So AuNPs are gradually applied to fabricate glucose biosensors in the field of electroanalysis [9,10]. AuNPs were often combined with other nanomaterials such as carbon nanotubes [22], graphene [23] and inorganic nanomaterials [24] for GOD loading. Ordered mesoporous carbon (OMC) could be deemed as such a good candidate owing to the extremely uniform pore structure, large specific pore volume, high specific surface area and biocompatibility [14–17]. A sensitive glucose biosensor with ferrocenecarboxylic mediator on GOD/2D-CMM/GCE was reported [14]. Nafion/GOD–OMCs/GE showed good analytical behavior of glucose [17]. In order to accelerate electron transfer between GOD and the electrode, it is necessary to synthesize new nanomaterials as GOD supporter. Therefore, it will be interesting for immobilizing GOD on ordered mesoporous carbon–Au nanoparticles (OMC–Au) nanocomposites to investigate the performance of this glucose biosensor.

In this work, AuNPs were deposited on OMC by one-step reaction with $NaBH_4$ as reductant and sodium citrate as stabilizer in aqueous solution. The unique structure of OMC allows for the obtainment of highly dispersed AuNPs on the outer surface. A glucose biosensor based on the DET of GOD was fabricated by immobilizing GOD onto OMC–Au nanocomposites. The biosensor displays the advantages of easy construction and efficiently preserved bioactivity of the GOD. Moreover, it also exhibits significant

* Corresponding author. Tel.: +86 0431 85099762; fax: +86 0431 85099762.
E-mail address: guolp078@nenu.edu.cn (L. Guo).

0039-9140/$ – see front matter © 2010 Elsevier B.V. All rights reserved.
doi:10.1016/j.talanta.2010.11.022

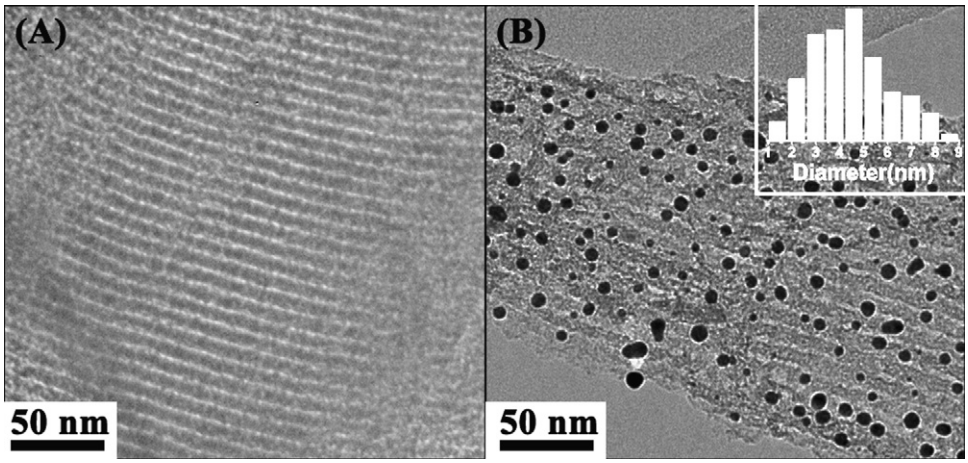

Fig. 1. The TEM images of the OMC (A) and the OMC–Au (B), inset of (B) is Au particle size distribution.

improved performances connected with faster electron transfer, high sensitivity and good stability.

2. Experimental

2.1. Reagents and apparatus

Pluronic P123 (non-ionic triblock copolymer, $EO_{20}PO_{70}EO_{20}$) and hydrogen tetrachloroaurate(III) trihydrate ($HAuCl_4{\cdot}3H_2O$, 99.9%) were purchased from Sigma–Aldrich. Glucose oxidase (GOD, EC. 1.1.3.4, lyophilized powder, 151 U mg^{-1}, from Aspergillus niger) was obtained from Sigma. D-Glucose was obtained from Beijing Chemical Company (Beijing, China) and the freshly prepared D-glucose solution was allowed to come to mutarotation equilibrium by standing overnight. All other chemicals were of analytical grade and were used without further purification. Phosphate buffer solutions (0.1 M PBS) with different pH (3.0, 4.0, 5.0, 6.0, 7.0, 8.0, 9.0 and 10.0) were prepared by mixing the stock solution of NaH_2PO_4 and Na_2HPO_4.

TEM images were obtained using a JEM-2100F transmission electron microscope (JEOL, Japan) operating at 200 kV. X-ray energy-dispersive spectroscopy (EDS) was conducted on a Philips XL-30 field-emission scanning electron microscope operated at 20 kV. Quantitative analysis of elements was measured by EDS. X-ray diffraction (XRD) patterns were obtained on an X-ray D/max-2200vpc (Rigaku Corporation, Japan) instrument operated at 40 kV and 20 mA and using Cu Kα radiation (λ = 0.15406 nm). The cyclic voltammetry (CV) and differential pulse voltammetry (DPV) were performed with a CHI660C electrochemical workstation (CH Instruments, China) in a conventional three-electrode cell. Glass carbon (GC) electrode (3 mm diameter) or a modified GC electrode served as a working electrode, whereas an Ag/AgCl (in saturated KCl solution) and a platinum wire served as the reference and counter electrodes, respectively.

2.2. Syntheses of OMC and OMC–Au nanocomposites

The silica templates (SBA-15) were synthesized using Pluronic P123 as the surfactant and tetraethyl orthosilicate as the silica source [25]. OMC was prepared according to the method reported by Ryoo et al. [17].

A chemical reduction method was used to prepare OMC–Au nanocomposites [26,27]. The prepared OMC (2 mg) was suspended in 0.1 wt.% $HAuCl_4$ solution (100 mL) by sonication for 24 h to obtain a good quality dispersed solution. 1 mL 1 wt.% sodium citrate was subsequently added to the suspended solution during stirring. After 1 min, freshly prepared 1 mL 0.075 wt.% $NaBH_4$ in 1 wt.% sodium citrate was quickly added to the solution under vigorously stirring. The reaction continued for 30 min until the color of the solutions did not change at room temperature. The black solid was separated by centrifuging at a speed of 4000 rpm, washed with deionized water for several times, and then dried overnight in an oven at 80 °C.

2.3. Fabrication of GOD/OMC–Au/GC electrode

Prior to use, GC electrode was successively polished with 1.0, 0.3, and 0.05 μm alumina powders, respectively, rinsed thoroughly with doubly distilled water between each polishing step, then washed successively with 1:1 nitric acid, acetone and doubly distilled water in ultrasonic bath and dried in air. The film electrode was prepared by a simple casting method. As-prepared OMC–Au nanocomposites (1 mg) were dispersed to 1 mL dimethylformamide (DMF) and it was sonicated for 1 h to form a stable black suspension (the concentration of OMC–Au, 1.0 mg mL^{-1}). 5 μL of OMC–Au nanocomposites were dropped onto the cleaned GC electrode surface and dried under an infrared lamp. Then the OMC–Au modified GC electrode was immersed into the solution of GOD (10 mg mL^{-1}, 0.1 M PBS (pH 7.0)) about 24 h at 4 °C in refrigerator. Finally, the GOD/OMC–Au/GC electrode was rinsed throughout with double distilled water to wash away the loosely adsorbed enzyme molecules. For comparison, the GOD/OMC/GC and GOD/GC electrodes were also prepared by the same procedure. Those enzyme-modified electrodes were stored at 4 °C in refrigerator when not in use.

2.4. Electrochemical measurements of glucose

Glucose measurements were carried out in 0.1 M pH 7.0 PBS at room temperature by CV or DPV. For the measurement of glucose, the proper amount of glucose was transferred into the oxygen-saturated 0.1 M pH 7.0 PBS (5.0 mL). The current response due to the addition of glucose was recorded. Voltammograms were recorded from −0.7 to −0.2 V at scan rate of 0.10 V s^{-1}. The parameters of DPV are: pulse amplitude: 0.05 V; pulse width: 0.05 s; pulse period: 0.2 s.

3. Results and discussion

3.1. Characterization of OMC–Au nanocomposites

The TEM images of OMC (Fig. 1A) and OMC–Au (Fig. 1B) are shown in Fig. 1. The OMC shows the ordered structure (Fig. 1A).

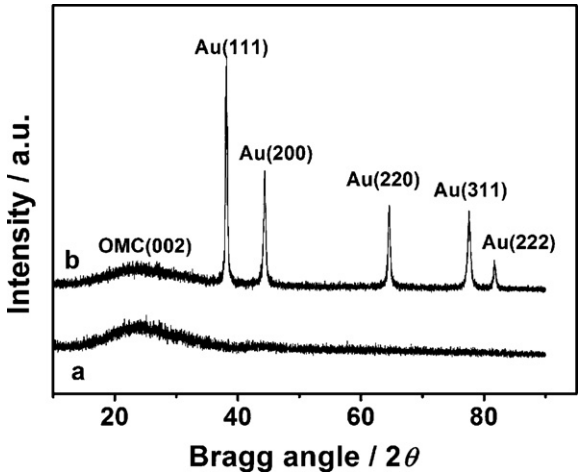

Fig. 2. XRD patterns of OMC (a) and OMC–Au (b).

One can note that the ordered structure is not very affected by the presence of AuNPs (Fig. 1B). Compared with Fig. 1A, the highly dispersed AuNPs with the size of 1.1–8.7 nm are observed on outer surface of OMC (Fig. 1B). The mean diameter of AuNPs is 4.4 nm (inset of Fig. 1B). EDS is used to identify and characterize semi-quantitatively, chemical elements present on surface of substance. The loading amount of AuNPs on the surface of OMC was measured by EDS, which is nearly 17 wt.%.

XRD patterns of OMC and as-prepared OMC–Au nanocomposites are shown in Fig. 2. The broad diffraction peak at around $2\theta = 23^{\circ}$ is attributed to the (0 0 2) diffraction of graphite (Fig. 2). Compared with the XRD analysis of OMC (Fig. 2, curve a), the OMC–Au nanocomposites (Fig. 2, curve b) show five peaks assigning to the (1 1 1), (2 0 0), (2 2 0), (3 1 1), and (2 2 2) crystalline plane diffraction of the AuNPs, respectively, indicating an evident face-centered cubic (fcc) Au crystal structure (JCPDF04-0784). The average diameter of AuNPs is 4.4 nm calculated by Scherrer formula from the half-width of the (2 0 0) diffraction peak, which is in good agreement with the result from the TEM image.

3.2. Direct electrochemistry of the GOD on the OMC–Au/GC electrode

Fig. 3 shows the CVs of different electrodes in nitrogen-saturated 0.1 M PBS (pH 7.0). No redox peaks are observed at the bare GC (curve a), OMC/GC (curve c) and OMC–Au/GC (curve d) electrodes, indicating that no redox reaction is undergone. Meanwhile, it can be seen that the background current of OMC–Au/GC electrode is higher than that of the OMC/GC and bare GC electrodes. This may be ascribed to the good conductivity of AuNPs. In Fig. 3, except the GOD/GC electrode (curve b), the GOD/OMC/GC (curve e) and GOD/OMC–Au/GC (curve f) electrodes show a couple of well-defined, quasi-reversible redox peaks, corresponding to the DET of the immobilized GOD. This indicates that the OMC or OMC–Au can facilitate the direct electrochemistry of the redox-active site of GOD (the conversion of FAD/$FADH_2$ center) without the help of the electron transfer mediators. Besides, the peak currents of GOD/OMC–Au/GC electrode are higher than those of GOD/OMC/GC electrode. Comparison between GOD/OMC/GC electrode and GOD/OMC–Au/GC electrode reveals that the existence of AuNPs accelerates the direct electron communication between the electroactive sites embedded in enzyme and the electrode. This may be attributed to the good conductivity and biocompatibility of AuNPs.

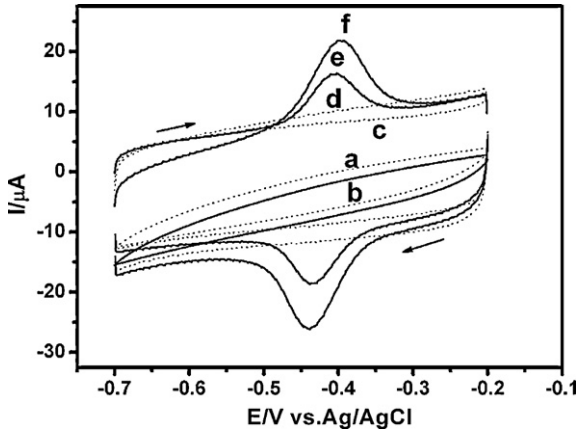

Fig. 3. CVs of bare GC (a), GOD/GC (b), OMC/GC (c), OMC–Au/GC (d), GOD/OMC/GC (e) and GOD/OMC–Au/GC (f) electrodes in 0.1 M nitrogen-saturated PBS (pH 7.0) at the scan rate of 100 mV s^{-1}.

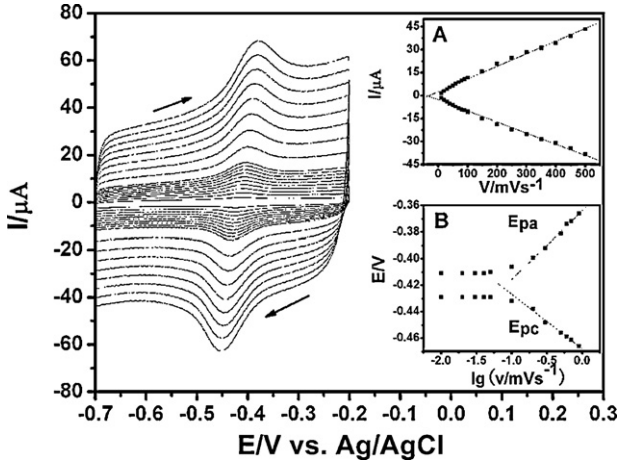

Fig. 4. CVs of GOD/OMC–Au/GC electrode with different scan rate in nitrogen-saturated 0.1 M PBS (pH 7.0). Inset A: plots of peak currents vs. scan rate. Inset B: plots of the anodic peak potential (E_{pa}), and cathodic peak potential (E_{pc}) vs. the logarithm of the scan rate.

Additionally, the surface coverage (Γ) of GOD was estimated according to $\Gamma = Q/nFA$ [28], where Q is the charge involved in the reaction, n is the number of the electron transferred, A is the geometric area of the working electrode, F is the Faraday constant, and Γ is the surface concentration of the electroactive substance. The Γ value of GOD/OMC–Au/GC electrode was calculated to be 2.99×10^{-9} mol cm^{-2}, which is much larger than that of GOD/OMC/GC electrode (1.80×10^{-9} mol cm^{-2}). Moreover, such a surface coverage is larger than that of gold nanoparticles modified carbon paste electrode (9.8×10^{-12} mol cm^{-2}) [8], GOx/Pt-CMM (2.2×10^{-10} mol cm^{-2}) [14] and GOD-IL–GNP-IL–SWNT/GCE (1.27×10^{-10} mol cm^{-2}) [29]. This demonstrates that the OMC–Au nanocomposites can provide a favorable microenvironment for enzyme immobilization and greatly retain the activity of GOD. These prove that the GOD/OMC–Au/GC electrode is more beneficial to the direct electrochemistry of GOD than the GOD/OMC/GC and some other electrodes.

Fig. 4 shows the typical CVs of GOD/OMC–Au/GC electrode in 0.1 M PBS (pH 7.0) with scan rate from 10 to 500 mV s^{-1}. The anodic peak current (i_{pa}) and cathodic peak current (i_{pc}) are linearly proportional to the scan rate (ν) in the range from 10 to 500 mV s^{-1} (Fig. 4, inset A). Linear regression equations:

$$i_{pa} = 2.53 + 0.083\nu \quad (r = 0.997);$$

$$i_{pc} = -2.70 - 0.073\nu \quad (r = -0.997).$$

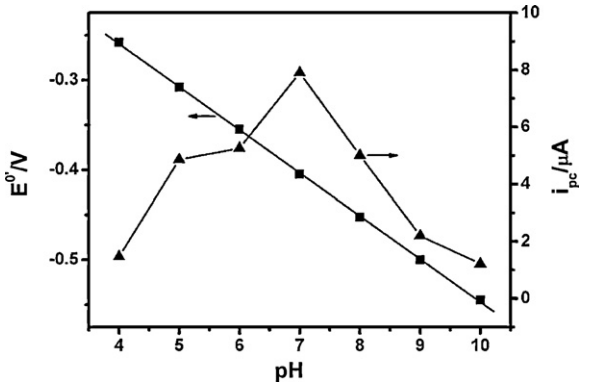

Fig. 5. Influence of pH on the cathodic peak current (i_{pc}) and formal potential ($E^{0\prime}$) of GOD/OMC–Au/GC electrode.

The equations indicate that the electrode process is surface-controlled quasi-reversible process.

With the increase of scan rate, the oxidation peak shifts to more positive value and the reduction peak to more negative value with the peak-to-peak separation (ΔE_p) increasing gradually. There is a linear relationship between E_p and lg ν (Fig. 4 inset B), the regression equations are

$$E_{pa} = -0.36 + 0.052 \lg \nu \quad (r = 0.996);$$

$$E_{pc} = -0.47 - 0.041 \lg \nu \quad (r = -0.996).$$

According to the Laviron's equation [30], the electron transfer coefficient α was evaluated to be 0.43 and the apparent heterogeneous electron transfer rate constant (k_s) was estimated as 5.03 s^{-1} at the GOD/OMC–Au/GC electrode, which is much higher than that of GOD-IL–GNP-IL–SWNT/GCE (2.12 s^{-1}) [29], GOD–graphene–chitosan/GCE (3.01 s^{-1}) [31], GOD/Cys/AuNPs/ITO (3.70 s^{-1}) [10] and Nafion/GOD–MC–FDU-15/GC (4.095 s^{-1}) [12]. At the same condition (data not shown), the k_s of GOD/OMC/GC electrode was also calculated as 3.30 s^{-1}. These further prove that the existence of AuNPs facilitates the electron exchange between redox-active sites of GOD and the electrode.

The pH value of the solution has influence on the electrochemical behavior of GOD. The effect of solution pH on the DET of GOD/OMC–Au/GC electrode was studied in Fig. 5. With rising of pH value, the cathodic peak currents increase and reach a maximum at pH 7.0 and then decrease with further increasing, which is ascribed to the higher activity of GOD in neutral solution. The formal potential $E^{0\prime}$ shows a linear relativity to the buffer pH value from 4.0 to 10.0 with a slope of −48.0 mV/pH (r = 0.999) (Fig. 5). This value is close to the theoretical −58.6 mV/pH for a reversible coupled two-electron and two-proton transfer electrochemical process according to the reaction shown in Eq. (1) [8]:

$$\text{GOD-FAD} + 2e^- + 2H^+ \leftrightarrow \text{GOD-FADH}_2 \quad (1)$$

All of these indicate that two electrons ($2e^-$) and two protons ($2H^+$) participate in the direct electrochemical reaction of GOD immobilized on OMC–Au/GC electrode.

3.3. Detection of glucose based on direct electrochemistry at GOD/OMC–Au/GC electrode

As shown in Fig. 6, the effect of the dissolved oxygen on the electrochemical behavior of the GOD/OMC–Au/GC electrode was studied. A pair of well-defined, quasi-reversible redox peaks is observed in nitrogen-saturated (curve a) PBS (pH 7.0) in Fig. 6. Compared to curve a, the reduction peak current of GOD significantly increases and oxidation peak current decreases in the presence of

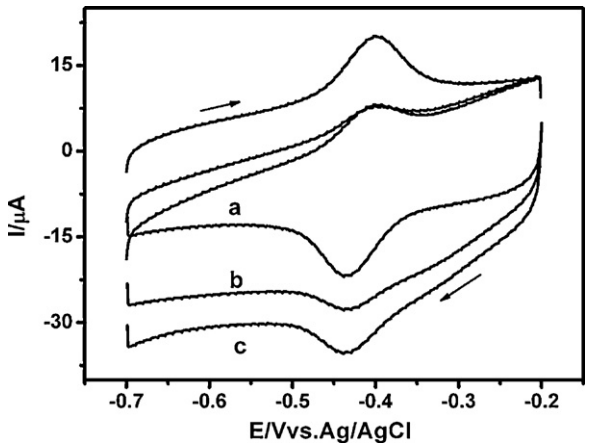

Fig. 6. CVs of the GOD/OMC–Au/GC electrode in 0.1 M nitrogen-saturated (a), 1.0 mM glucose oxygen-saturated (b) and oxygen-saturated (c) PBS (pH 7.0) at a scan rate of 100 mV s^{-1}.

oxygen (curve c) at the GOD/OMC–Au/GC electrode, indicating that GOD on the film can nicely catalyze the oxygen reduction according to Eqs. (1) and (2) [8]:

$$\text{GOD-FADH}_2 + O_2 \rightarrow \text{GOD-FAD} + H_2O_2 \quad (2)$$

Moreover, when glucose was added into oxygen-saturated PBS, the reduction current decreased at the GOD/OMC–Au/GC electrode (Fig. 6, curve b). Meanwhile, the enzyme-catalyzed reaction occurred according to Eq. (3) [8], and decreased the amount of GOD on the electrode surface.

$$\text{Glucose} + \text{GOD(FAD)} \rightarrow \text{Gluconolactone} + \text{GOD(FADH}_2) \quad (3)$$

Thus, the addition of glucose restrains the electrocatalytic reaction, which leads to the decrease of reduction current [32]. With the increasing of glucose concentration, the reduction current gradually decreases. This could be employed to fabricate a glucose biosensor.

The performance of the GOD/OMC–Au/GC electrode toward glucose response was investigated by DPV in oxygen-saturated 0.1 M PBS (pH 7.0) upon addition of glucose (Fig. 7). The peak at −0.4 V was ascribed to the reduction of FAD. The reduction current of FAD linearly diminishes with the glucose concentration rising. As is shown in Fig. 7, inset A, the response current is linear to the concentration of glucose over the range from 0.05 to 0.3 mM (r = 0.998) in

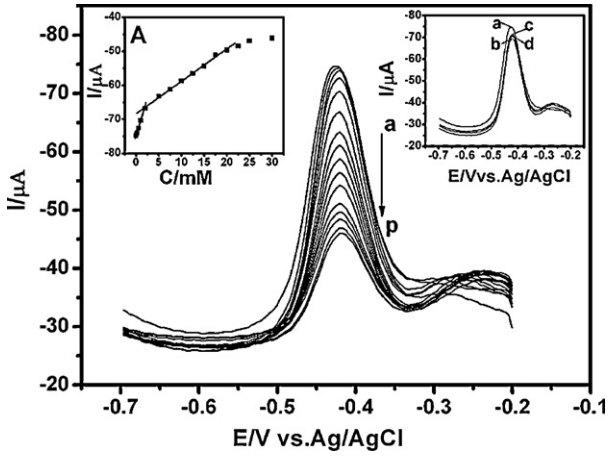

Fig. 7. DPVs of different concentration glucose (a–p from 0 to 30 mM) at the GOD/OMC–Au/GC electrode in oxygen-saturated 0.1 M PBS (pH 7.0). Inset A: calibration curve; inset B: DPVs of 0 mM glucose (a), 1.0 mM glucose (b), 1.0 mM glucose + 0.1 mM AA (c) and 1.0 mM glucose + 0.1 mM UA (d). Scan rate: 100 mV s^{-1}.

Table 1
Comparison of analytical performance of some glucose biosensors.

Glucose sensor (mM)	Linear range	Sensitivity ($\mu A\,mM^{-1}$)	K_M^{app} (mM)	Stability (i_n/i_i)[e] %	Reference
GOD/OMC–Au/GC	0.05–0.3	4.34	0.60	30 days (88%)	This work
	0.3–20	0.96			
Nafion/GOx/OMC/GC	0.5–15	0.053	–	30 days (93%)	[16]
Chitosan/GOx/CNTs[a]/GC	0–7.8	0.52	8.2	–	[7]
GOD/graphene/chitosan/GC	0.08–12	2.69[f]	4.4	–	[31]
GOD/Cys[b]/AuNPs/ITO	0.04–4.8	–	12.1	35 days (85%)	[10]
PDDA[c]–GOD/Au/CNT/GC	0.5–5.0	2.50	1.76	7 days (97%)	[34]
Au–GS[d]–GOx–Nafion/GC	0.015-5.8	–	4.4	21 days (90%)	[23]
Pt/CMK-3–GOx–gelatin/GC	0.04–12	1.79	10.8	30 days (95%)	[35]
TiO_2/GOD/nafion/GC	0.15–1.2	0.3	–	14 days (94%)	[36]
Nafion/GOx/ZnO/gold electrode	0.02–4.5	0.12[f]	2.19	–	[37]

[a] Carbon nanotubes.
[b] L-Cysteine.
[c] Poly(diallydimethylammonium) chloride.
[d] Sulfonated graphene.
[e] The proportion of now current and initial current.
[f] The value was calculated by the experiment data of the reference.

lower concentration region, and from 0.3 to 20 mM ($r = 0.998$) in the higher concentration region. The equations of the calibration plots are:

$$I(\mu A) = -68.36 + 0.954C(mM) \quad (r = 0.998)$$

$$I(\mu A) = -74.71 + 4.341C(mM) \quad (r = 0.998)$$

Therefore, the sensitivity of the GOD/OMC–Au/GC electrode was calculated to be 4.34 $\mu A\,mM^{-1}$ and 0.96 $\mu A\,mM^{-1}$ in lower and higher concentration region, respectively, which is much higher than that of some other glucose biosensors reported in literatures [7,16] (see Table 1).

The reduction current reaches a minimum value at the higher glucose concentration in the inset A of Fig. 7, exhibiting typical Michaelis–Menten kinetic behaviors. The apparent Michalis–Menten constant (K_M^{app}), which gives an indication of the enzyme-substrate kinetics, is used to evaluate the biological activity of the immobilized enzyme. The value of K_M^{app} can be calculated from the Lineweaver–Burk equation [33]:

$$\frac{1}{I_{SS}} = \frac{1}{I_{max}} + \frac{K_M^{app}}{I_{max}C} \quad (4)$$

where I_{SS} is the steady-state current after the addition of substrate, I_{max} is the maximum current measured under saturated substrate condition and C is the bulk concentration of the substrate. The value of K_M^{app} was calculated as 0.6 mM on the GOD/OMC–Au/GC electrode, which was smaller than some reported values [10,23,34]. The smaller K_M^{app} of GOD on GOD/OMC–Au/GC electrode indicates that the enzyme electrode possesses higher enzymatic activity and affinity to glucose.

A further comparison of the obtained results to other glucose biosensors based on other nanomaterials was summarized in Table 1. These nanomaterials include carbon nanotubes, graphene, gold nanoparticles, and semiconductor metal oxides nanomaterials. From Table 1, one can conclude that the proposed biosensor has a higher sensitivity and a better linear range than those previous reported papers. The good catalytic response to glucose implies that OMC–Au nanocomposites provide a good biocompatible microenvironment for maintaining enzymatic activity. It can be also concluded that the value of K_M^{app} is quite low in comparison with those obtained at other glucose biosensors from Table 1. This may be attributed to the more active sites of OMC–Au nanocomposites with low transport limitations of substrate, which make the enzyme contact with substrate easier and facile the electron transport.

3.4. Selectivity of the biosensor

We investigated the interference effect of ascorbic acid (AA), uric acid (UA), towards the glucose using DPV method. As shown in inset B of Fig. 7, 0.1 mM AA (curve c) and 0.1 mM UA (curve d) caused an increase of 1.6% or 2.5% in the reduction current of 1.0 mM glucose, respectively. This result indicated a good selectivity of the biosensor. Owing to the low operating potential, those coexisted electroactive substances had not interfered in glucose [38].

To illustrate feasibility of the composite modified electrode in practical analysis, the GOD/OMC–Au/GC electrode was used to detect glucose in human blood (from local hospital) by utilizing standard addition method. The results obtained are shown in Table 2. The average recovery is 99.97% and 100.2%, respectively. The results were satisfactory and agreed closely with those detected by the hospital.

3.5. Reproducibility and stability of the biosensor

The reproducibility and stability of the proposed biosensor were also investigated. The relative standard deviation (RSD) was 3.4% at the GOD/OMC–Au/GC electrode by five successive measurements

Table 2
Results for determinations of glucose in human blood samples ($n = 3$).

Sample	Added (mM)	Expected (mM)	Found (mM)	Recovery (%)	Mean recovery (%)
Sample 1	0	–	1.68	–	99.97
	2.00	3.68	3.71	101.50	
	4.00	5.68	5.65	99.25	
	6.00	7.68	7.63	99.17	
Sample 2	0	–	3.35	–	100.2
	1.00	4.35	4.40	100.5	
	3.00	6.35	6.34	99.67	
	5.00	8.35	8.37	100.4	

at a glucose concentration of 1.0 mM. For five different and freshly made independently under the same conditions, the RSD was 5.2%. These demonstrate an acceptable repeatability in the construction of biosensor. The stability of electrode was determined by storing the sensor at 4 °C for 30 days. After 30 days, the redox peak currents of GOD retain 88% and 74% of their initial response values on the GOD/OMC–Au/GC and GOD/OMC/GC electrodes, respectively. The stability of electrode was also investigated by examining the cyclic voltammetric peak currents of GOD after continuously scanning for 50 cycles. There was nearly no obvious decrease of the voltammetric response on GOD/OMC–Au/GC electrode, which proves that the enzyme electrode is stable in buffer solution. In contrast, the voltammetric response lost 9% of the initial values on GOD/OMC/GC electrode. These indicate that the GOD/OMC–Au/GC electrode has better stability than GOD/OMC/GC electrode. The good stability of the GOD/OMC–Au/GC electrode may be attributed to the good biocompatibility of the OMC–Au nanocomposites which offer a friendlier microenvironment for GOD to retain its bioactivity.

4. Conclusion

In this work, the OMC–Au nanocomposites have been successfully synthesized by using rapid and convenient one-step method. More important, AuNPs can be well-defined deposited on the OMC due to the premixing of OMC with $HAuCl_4$ solution. OMC–Au nanocomposites were used to construct a mediator-free glucose biosensor. Due to the excellent biocompatibility of the OMC–Au nanocomposites, the direct electrochemistry of GOD was performed successfully and the immobilized GOD retained its bioactivity. The fabricated glucose biosensor displays high sensitivity, good stability and acceptable reproducibility. The OMC–Au nanocomposites also provide a promising platform for the development of other biosensors.

Acknowledgment

The authors gratefully acknowledge the financial support by the National Natural Science Foundation of China (No. 20875012).

References

[1] J.E. Frew, H.A.O. Hill, Eur. J. Biochem. 172 (1988) 261–269.
[2] A. Guiseppi-Elie, C.H. Lei, R.H. Baughman, Nanotechnology 13 (2002) 559–563.
[3] J.J. Gooding, R. Wibowo, J. Liu, W. Yang, D. Losic, S. Orbons, F.J. Mearns, J.G. Shapter, D.B. Hibbert, J. Am. Chem. Soc. 125 (2003) 9006–9007.
[4] M.G. Zhang, A. Smith, W. Gorski, Anal. Chem. 76 (2004) 5045–5050.
[5] A. Kaushik, R. Khan, P.R. Solanki, P. Pandey, J. Alam, S. Ahmad, B.D. Malhotr, Biosens. Bioelectron. 24 (2008) 676–683.
[6] M.E. Ghica, R. Pauliukaite, O. Fatibello-Filho, C.M.A. Brett, Sens. Actuators B 142 (2009) 308–315.
[7] Y. Liu, M.K. Wang, F. Zhao, Z.A. Xu, S.J. Dong, Biosens. Bioelectron. 21 (2005) 984–988.
[8] S.Q. Liu, H.X. Ju, Biosens. Bioelectron. 19 (2003) 177–183.
[9] Y.H. Wu, S.S. Hu, Bioelectrochemistry 70 (2007) 335–341.
[10] J.W. Wang, L.P. Wang, J.W. Di, Y.F. Tu, Sens. Actuators B 135 (2008) 283–288.
[11] M.H. Asif, S.M. Usman Ali, O. Nur, M. Willander, C. Branmark, P. Stralfors, U.H. Englund, F. Elinder, B. Danielsson, Biosens. Bioelectron. 25 (2010) 2205–2211.
[12] K.Q. Wang, H. Yang, L. Zhu, Z.S. Ma, S.Y. Xing, Q. Lv, J.H. Liao, C.P. Liu, W. Xing, Electrochim. Acta 54 (2009) 4626–4630.
[13] Z.H. Dai, J.C. Bao, X.D. Yang, H.X. Ju, Biosens. Bioelectron. 23 (2008) 1070–1076.
[14] C.P. You, X. Xu, B.Z. Tian, J.L. Kong, D.Y. Zhao, B.H. Liu, Talanta 78 (2009) 705–710.
[15] L.D. Zhu, C.Y. Tian, D.X. Zhu, R.L. Yang, Electroanalysis 20 (2008) 1128–1134.
[16] M. Zhou, L. Shang, B.L. Li, L.J. Huang, S.J. Dong, Biosens. Bioelectron. 24 (2008) 442–447.
[17] S. Jun, S.H. Joo, R. Ryoo, M. Kruk, M. Jaroniec, Z. Liu, T. Ohsuna, O. Terasaki, J. Am. Chem. Soc. 122 (2000) 10712–10713.
[18] M.C. Daniel, D. Astruc, Chem. Rev. 104 (2004) 293–346.
[19] S.Q. Liu, D Leech, H.X. Ju, Anal. Lett. 36 (2003) 1–19.
[20] X. Luo, J. Xu, Y. Du, H. Chen, Anal. Biochem. 334 (2004) 284–289.
[21] H.R. Luckarift, D. Ivnitski, R. Rincon, P. Atanassov, G.R. Johnson, Electroanalysis 22 (2010) 784–792.
[22] B.Y. Wu, S.H. Hou, F. Yin, Z.X. Zhao, Y.Y. Wang, X.S. Wang, Q. Chen, Biosens. Bioelectron. 22 (2007) 2854–2860.
[23] K.F. Zhou, Y.H. Zhu, X.L. Yang, C.Z. Li, Electroanalysis 22 (2010) 259–264.
[24] H.C. Wang, X.S. Wang, X.Q. Zhang, X. Qin, Z.X. Zhao, Z.Y. Miao, N. Huang, Q. Chen, Biosens. Bioelectron. 25 (2009) 142–146.
[25] D. Zhao, J. Feng, Q. Huo, N. Melosh, G.H. Fredrickson, B.F. Chmelka, G.D. Stucky, Science 279 (1998) 548–552.
[26] D. Du, M.H. Wang, J. Cai, Y.H. Qin, A.D. Zhang, Sens. Actuators B 143 (2010) 524–529.
[27] K.R. Brown, A.P. Fox, M.J. Natan, J. Am. Chem. Soc. 118 (1996) 1154–1157.
[28] A.J. Bard, L.R. Faulkner, Electrochemical Methods: Fundamentals and Applications, 2nd ed., John Wiley & Sons, New York, 2001.
[29] R.F. Gao, J.B. Zheng, Electrochem. Commun. 11 (2009) 608–611.
[30] E. Laviron, J. Electroanal. Chem. 101 (1979) 19–28.
[31] X.H. Kang, J. Wang, H. Wu, I.A. Aksay, J. Liu, Y.H. Lin, Biosens. Bioelectron. 25 (2009) 901–905.
[32] C.Y. Deng, J.H. Chen, X.L. Chen, C.H. Xiao, L.H. Nie, S.Z. Yao, Biosens. Bioelectron. 23 (2008) 1272–1277.
[33] R.A. Kamin, G.S. Wilson, Anal. Chem. 52 (1980) 1198–1205.
[34] L.Y. Yao, K.K. Shiu, Electroanalysis 20 (2008) 1542–1548.
[35] J.J. Yu, D.L. Yu, T. Zhao, B.Z. Zeng, Talanta 74 (2008) 1586–1591.
[36] S.J. Bao, C.M. Li, J.F. Zang, X.Q. Cui, Y. Qiao, J. Guo, Adv. Funct. Mater. 18 (2008) 591–599.
[37] J.X. Wang, X.W. Sun, A. Wei, Y. Lei, X.P. Cai, C.M. Li, Z.L. Dong, Appl. Phys. Lett. 88 (2006) 2331061–2331063.
[38] B. Wolfrum, M. Zevenbergen, S. Lemay, Anal. Chem. 80 (2008) 972–977.